Palaeogeography, Palaeoclimatology, Palaeoecology 562 (2021) 109952

Contents lists available at ScienceDirect

Palaeogeography, Palaeoclimatology, Palaeoecology

journal homepage: www.elsevier.com/locate/palaeo

Changes in sea surface hydrography and productivity in the western equatorial Atlantic since the last interglacial

Patricia Piacsek[a,*], Hermann Behling[b], Fang Gu[b], Igor Martins Venancio[a,c], Douglas V.O. Lessa[a], Andre Belem[d], Ana Luiza S. Albuquerque[a]

[a] Geochemistry Graduate Program, Fluminense Federal University, Niterói, Brazil
[b] University of Goettingen, Department of Palynology and Climate Dynamics, Goettingen, Germany
[c] Center for Weather Forecasting and Climate Studies (CPTEC), National Institute for Space Research (INPE), Cachoeira Paulista, Brazil
[d] PPG Oceans and Earth Dynamics, Federal Fluminense University, Niterói, Brazil

ARTICLE INFO

Keywords:
Dinoflagellate
Glacial-Interglacial
Intertropical Convergence Zone
Heinrich Stadials

ABSTRACT

Scientific projections point to the increase of greenhouse gas levels in the atmosphere will turn the oceans warmer and, consequently, the upper layer of the thermohaline circulation will get thicker, restricting the productivity areas. Oligotrophic conditions will tend to prevail, and expanding the range of proxy data in oligotrophic oceans, across different climate scenarios, has the potential to improve predictions of climate models about how primary productivity will respond. Still, the variability of past primary production in the equatorial Atlantic remains elusive. We used organic-walled dinoflagellate cysts (dinocysts) assemblages to reconstruct changes in the sea surface hydrography and productivity in the western equatorial Atlantic over the last ~130 kyr. Four dinocysts assemblages were defined: open ocean, river outflow, neritic and nutricline assemblages. Multiple proxies were used to support the environmental changes evidenced by the observed variations in the dinocyst assemblages, such as the X-ray fluorescence (XRF) Ti/Ca ratio, and planktonic foraminifera abundances. We observed glacial-interglacial as well as the millennial-scale changes in the dinocyst assemblages. A clear glacial-interglacial pattern was marked by more autotrophs dinocysts over the interglacials and the prevalence of heterotrophs dinocysts during the glacial period. We pointed out the interchange of autotrophs assemblages (nutricline and open ocean) over the interglacials intervals, denoting divergences in nutrient availability. During the last glacial period, precipitation events occurred in northeastern Brazil due to southward displacements of the Intertropical Convergence Zone (ITCZ). The increase of precipitation boosted the freshwater input to the adjacent ocean, and the dinocyst assemblages oscillated in response to such freshwater/salinity changes. Over the glacial period, dinocysts with different nutritional requirements (autotrophs and heterotrophs) varied following the ITCZ displacements. Thus, in this study, we showed the influence of ocean-atmospheric processes on the ocean and investigated the productivity in an oligotrophic region over distinct past climatic backgrounds.

1. Introduction

Despite the relevance of more productive areas for the global carbon budget, the world's oceans have large-scale oligotrophic conditions. In a global warming scenario, oligotrophic regions of the oceans will tend to increase, as the warm upper layer of the thermohaline circulation will get thicker. Understand the responses of phytoplankton organisms in these regions over different climatic conditions has the potential to optimize climate simulations. The western equatorial Atlantic is characterized as a low productivity area, mainly due to the presence of the North Brazil Current (NBC) (Peterson and Stramma, 1991; Krauss, 1996). In this region, warm sea surface waters pile up and deepen the seasonal thermocline due to the modern dynamics of the trade winds (Hastenrath and Merle, 1987), denoting a nutrient-depleted surface layer, considered a quasí-permanent feature of the tropical and subtropical Atlantic (Herbland and Voituriez, 1979). Strong southeast (SE) trade winds create a thermocline tilt between the western and eastern equatorial Atlantic, with implications of the nutrient availability at the sea surface, setting the productivity regimes in both areas (Molinari et al., 1986).

Previous studies focusing on paleoceanographic reconstructions have shown that the transport of warm waters to the western equatorial Atlantic was reduced during the phase with weak SE trades winds, consequently attenuating the east-west thermocline tilt (Wolff et al.,

* Corresponding author at: Departamento de Geoquímica, Universidade Federal Fluminense, Outeiro São João Baptista s/n, Centro Niterói, RJ, Brazil.
E-mail address: Piacsekpatricia@gmail.com (P. Piacsek).

https://doi.org/10.1016/j.palaeo.2020.109952
Received 20 February 2020; Received in revised form 9 July 2020; Accepted 2 August 2020
Available online 17 October 2020

1999; Venancio et al., 2018). Oscillations in the thermocline thickness possibly influenced past productivity by modulating the nutrients diffusion into the photic zone. Indeed, several studies indicate that glacial-interglacial changes in productivity occurred in the region, with higher productivity during interglacials compared to glacials (Rühlemann et al., 1996; Bickert et al., 1997; Mulitza et al., 1998; Kinkel et al., 2000; Vink et al., 2002).

The last glacial period exhibits singular environment conditions with lower relative sea-level (RSL) than the present, expanding the shoreline, and delivering more continental material to the ocean areas. Another particular feature was the intensification of the meridional temperature gradient between the North and the Tropical Atlantic, generating the compression of climatic zones towards the equator and driving stronger trade winds (Leroux, 1993; Parkin, 1974). In addition, displacements of the Intertropical Convergence Zone (ITCZ) generated changes in trade winds' direction and strength. Nevertheless, the southward shift of the ITCZ was accompanied by periods with weak southeast (SE) trade winds and intense precipitations events in northeastern Brazil. Rivers that flow into the ocean increased their freshwater and nutrients contribution due to more severe runoff, modulating the biological productivity in the western equatorial Atlantic (Vink et al., 2000).

Studies in different margins of the South Atlantic indicated that biological productivity could be reconstructed through organic-walled dinoflagellate cysts (dinocysts) (Hardy et al., 2016; Gu et al., 2017). In the western equatorial Atlantic, Portilho-Ramos et al., (2017) showed changes in stratification during millennial-scale events, triggered by the direct effect of precipitation over the ocean linked to ITCZ shifts. However, the authors did not focus on the impact of such stratification changes over primary productivity. Based on that, we aimed to reconstruct over a longer period, the influence of these changes in mixed layer depth in the productivity. Thus, an assessment of the impact of these distinct productivity-related processes during the past was still needed for this area. Oligotrophic regions comprise a vast portion of the oceans. In order to achieve greater accuracy in models that estimate the efficiency of primary productivity in the carbon cycle, it is important to understand the dynamics of primary productivity in oligotrophic regions. In this context, we aimed to evaluate the glacial-interglacial, millennial-scale changes in the sea surface hydrography and productivity, as well as the main processes linked to the observed variations at the western equatorial Atlantic over the last ~130 kyr.

2. Sediment core location and regional setting

The region is under the influence of different water masses, with the following vertical distribution: the North Atlantic Deep Water (NADW) in the range of 2.000–3.000 m deep, the Antarctic Intermediate Water (AAIW) established between 800 and 1.500 m deep, and the South Atlantic Central Water (SACW) which occupies the range of 200–500 m deep. The SACW flows between the AAIW and the Tropical Water (TW) at the surface layer (Stramma and England, 1999) (Fig. S1). Except for the southward flow of the NADW, the other water masses described (AAIW, SACW, TW) flow northward. At the surface layer, the NBC transports the TW, while the North Brazil Undercurrent (NBUC) flows

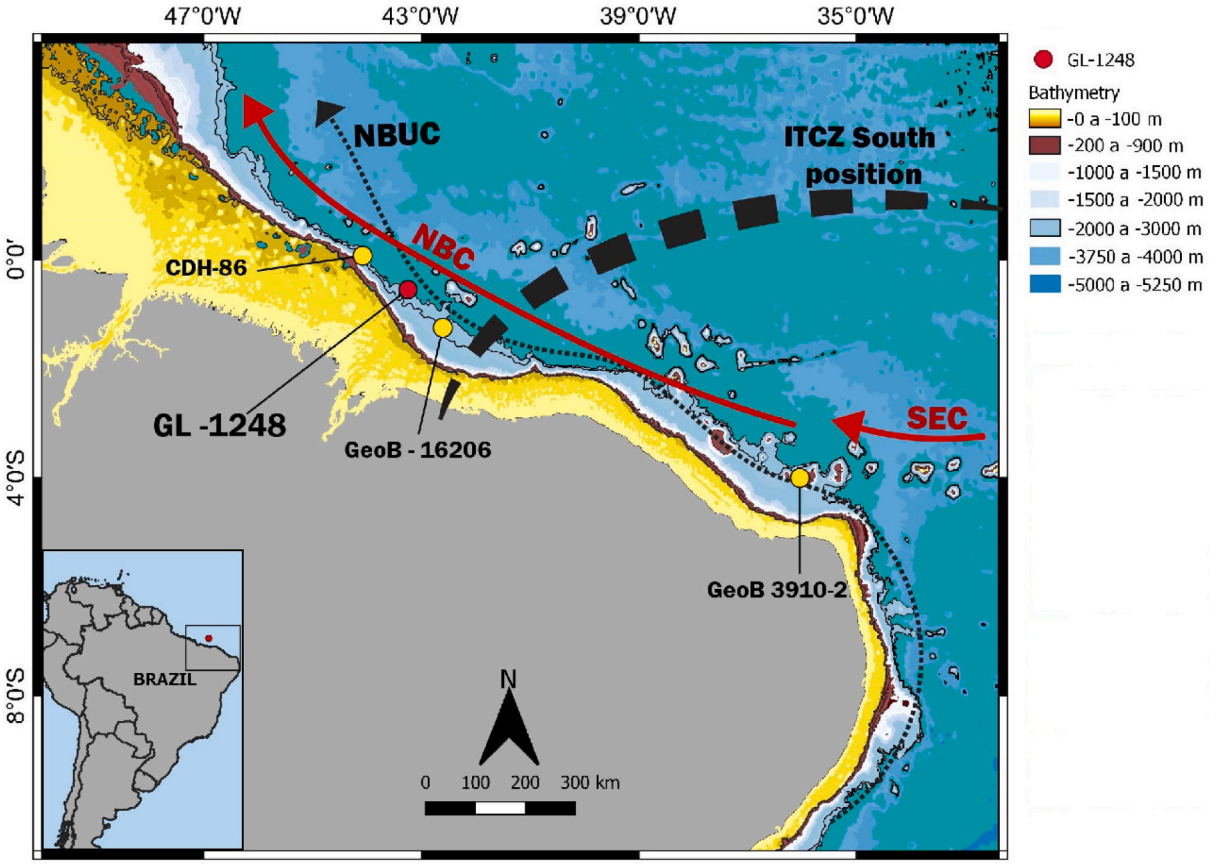

Fig. 1. Bathymetric map of the study area in northeastern Brazil and the location (red dot) of core GL-1248 (0°55.2′S, 43°24.1′W). Yellow dots represent other cores discussed in the text namely: CDH-86 (00°20.00′ N, 44°12.54′ W) (Nace et al., 2014), GeoB 16,206 (1°34.75′S 43°01.42′W) (Zhang et al., 2015), GeoB 3910–2 (4°15′ S 36°21′ W) (Dupont et al., 2010). The map also shows relevant surface currents such as the South Equatorial Current (SEC) and the North Brazil Current (NBC) in red arrows and the subsurface North Brazil Undercurrent (NBUC) in black dotted arrow. The dashed black line displays the approximate southern position of the Intertropical Convergence Zone (ITCZ) during austral summer (December–March). (For interpretation of the references to colour in this figure legend, the reader is referred to the web version of this article.)

at the sub-surface and within the thermocline layer, transporting the SACW (Stramma et al., 1995; Schott et al., 1995). The strength of NBC varies and is seasonally linked to the trade wind dynamics. During austral summer (December–March), the northeast (NE) trade winds gain strength, and NBC transport reduces (Stramma et al., 1995; Johns et al., 1998). As a result of intensifying NE trade winds, ITCZ reaches its southernmost position (2°S), leading to enhanced precipitation in northeastern Brazil (Hastenrath, 2012).

The marine sediment core GL-1248 (0° 55.2′ 55.2′S, 43° 24.1′ 24.1′W) was retrieved by Petrobras with a length of 19.29 m at 2264 m water depth, located at the slope of the Barreirinhas Bight on northeastern Brazil. The Barreirinhas Bight had a shallow continental shelf, ~75 m (m) below the sea surface (Mohriak, 2003; Krueger et al., 2012;), with a vertical gradient. The marine sediment core was about 160 km distance from the modern coastline (Fig. 1). The GL-1248 core was collected 280 km from the Parnaiba River fan and approximately 740 km from the Amazon River fan (Fig. S2). These geographical features assigned a high dynamic abiotic system with significant seasonal contrasts between the surface and subsurface salinity and nutrient loading, which are regulator factors of primary production (Mallin et al., 1993; Price et al., 2016).

3. Material and methods

3.1. Age model

The age model was established based on 12 AMS radiocarbon dates and the alignment of X-Ray fluorescence (XRF) Ti/Ca values with reference curves. The radiocarbon analysis was performed on planktonic foraminifera species *Globigerinoides ruber* (white) and *Trilobatus sacculifer* (planktonic foraminifera). The radiocarbon ages were used to generate a chronology for the upper 6.30 m of the core. The radiocarbon ages were calibrated with the IntCal13 calibration curve (Reimer et al., 2013). The chronology for the lower part of core GL-1248 (from ~5 m to ~17 m) was derived from tie points created between Ti/Ca alignment with the ice core $\delta^{18}O$ record from North Greenland Ice Core Project (Wolff et al., 2010). The downcore ages were modeled on the linear interpolation using the package Clam 2.2 (Blaauw, 2010). Venancio et al. (2018) described the age model of the marine core GL-1248 in detail. The Marine Isotopic Stages (MIS) boundaries and sub-divisions were defined according to Lisiecki and Raymo (2005). They were established as MIS 1 (starts at 14 kyr before present), MIS 3 (29–57 kyr), MIS 4 (57–71 kyr), MIS 5a (peak at 82 kyr), MIS 5b (peak at 87 kyr), MIS 5c (peak at 96 kyr), MIS 5d (peak at 109 kyr), MIS 5e (peak at 123 kyr).

3.2. Palynological preparation

A total of 131 samples were prepared for palynological analysis using standard laboratory procedures (Faegri and Iversen, 1989), but excluding acetolysis to preserve the dinocysts. About 4–6 g (wet weight) samples were prepared for dinoflagellate cysts analyses. At first, the sediment samples were sieved with a 150 μm mesh to remove the larger particles, such as shells and stones. After that, one tablet of exotic *Lycopodium clavatum* spores (containing 20,848 ± 1546 spores) was added to each sample to estimate the concentration (cysts/cm^3) and influx (cysts/cm^2/kyr) values (Stockmarr, 1971). Then, the samples were treated with hydrochloric acid (HCl, ca. 35%) for decalcification and cold hydrofluoric acid (HF, 40%) for siliceous content removal. After the chemical treatment, the samples went through an ultrasonic bath (maximum 30 s) for organic matter disaggregation. The samples were sieved with a 1 μm nylon mesh, but particles up to 5 μm may still pass through. The samples were processed at the Department of Palynology and Climate Dynamics, Georg-August-University Göttingen (Germany). Permanent microscope slides were made, and due to the low content, one to four slides per sample were counted. An average of 130 cysts was counted per sample (min. 83, max. 367). In total, 38 dinoflagellate cyst types were identified according to Zonneveld and Pospelova (2015) morphological descriptions. Dinoflagellate cysts were grouped into autotrophic and heterotrophic taxa due to the different energy resources (Gaines and Elbrächter, 1987; Taylor, 1987; Taylor et al., 2007). The most frequent taxa were presented in relative abundance and grouped based on their ecological affinities. The dinocysts influx (cysts/cm^2/kyr) was calculated by multiplying the dinocysts concentration (cysts/cm^3) with the sedimentation rate (cm/kyr), and the concentration was calculated for each sample following the Benninghoff (1962) equation.

3.3. Dinoflagellate cyst indexes

To evaluate the preservation condition of dinocysts in the marine environment, we calculated the degradation constant of sensitive cysts (k) and the reaction time (t). The kt index was obtained by the Eq. (1), with and X_f = final cyst concentration (cysts/cm^3) and X_i = initial cyst concentration (cysts/cm^3) (Zonneveld et al., 2007, 2010). The sensible oxygen cysts were designated as S-Cysts. The kt index was used to evaluate the selective degradation of the S-cysts (supplementary material, Table S1) in the marine sediments to reconstruct deep-ocean ventilation and infer if the sedimentary signal was modified by oxygen degradation (Zonneveld et al., 2007, 2010).

To indicate the heterotrophic and the autotrophic fluctuations through the last ~130 kyr, we used the ratio base on their relative abundances (H/A ratio) (Eq. (2)). Values close to number 1 indicated a more significant proportion of heterotrophic dinocysts (Pospelova and Kim, 2010). The dominance index was calculated using the Simpson index in Past3 software (Hammer et al., 2001).

Kt equation:

$$kt: \ln (X_i/X_f) \quad (1)$$

H/A ratio equation:

$$H/A\ ratio = H - cysts/(H\text{–}cysts + A\text{–}cysts) \quad (2)$$

3.4. Foraminifera assemblages

We analyzed the planktonic foraminifera assemblages with 4 cm resolution for MIS 1 to 5e sections due to a low sedimentation rate, and 10 cm for the other sections. The 10 cm^3 of sediment was washed through a 150 μm mesh sieve, and the residue material was dried at 50 °C for 24 h. The fraction larger than 150 μm was re-sieved dried and then divided until 300–500 individuals remained for identification at the species level. Species were identified by following the Kennett and Srinivasan (1983) and Loeblich and Tappan (1988) definitions.

3.5. Statistical analysis

To characterize the ecological affinities of dinocysts assemblages, we performed a Correspondence Analysis (CA). The CA added to each species disposition through the Axis due to its similarities (Legendre and Gallagher, 2001). The CA is a statistical ordination analysis better recommended to species with unimodal responses if compared to PCA, which is preferred for data with a linear distribution (Jongman et al., 1987; ter Braak and Prentice, 1988). For a better statistical measurement, regarding the samples with dinocyst taxa in low content, less than 5% were not taken into consideration. Unidentified species such as *Spiniferites* spp., *Operculadinium* spp., and *Impagidinium* spp. were also not considered, due to their controversial ecological affinities. Paleontological Statistics (Past3) software was used to perform CA statistical analysis (Hammer et al., 2001).

4. Results

4.1. Sedimentation rate, dinocyst concentrations, and the influx

The core GL-1248 covered the last ~130 kyr (MIS 1–5), with the mean sedimentation rate of 21 cm/kyr, with higher values during Marine Isotopic Stage (MIS) 3 (67 cm/kyr), and lower values during the Interglacials (~10 cm/kyr) (Fig. 2A). A total of 31 dinoflagellate cyst taxa were identified from 131 sediment samples. The dinocyst concentrations were generally low in GL-1248 (Fig. 2B), variating downcore from ~64 to 911 cysts/cm^3(averaging 249 cysts/cm^3). The influx values oscillated from 4.5 to 315 10^{2}cysts/cm^2/kyr (avg. 57 10^{2}cysts/cm^2/kyr) (Fig. 2C). Higher dinocysts concentration values were found during MIS 5 (~68 to 653 cysts/cm^3, avg. 244 cysts/cm^3), MIS 1 (~85 to 757 cysts/cm^3, avg. 242 cysts/cm^3), and during late MIS 3 (~64 to 911 cysts/cm^3, avg. 259 cysts/cm^3), periods of reduced sedimentation rate. The influx values during MIS 3 reached the highest values of the sediment core (~79.5 to 315 10^{2}cysts/cm^2/kyr, avg. 205 10^2 cysts/cm^2/kyr).

4.2. Dinoflagellate cyst indexes

The kt index showed an asynchronous pattern to the sedimentation rate. Our result indicated a relatively low degradation during the glacial (kt < 4, four is the critical value to evaluate the selective preservation in our record). The dominance index was weighted according to the abundance of the most common species (Fig. 2D). The *Brigantedinium* spp. was pacing the dominance index and, as a consequence, was the most frequent heterotrophic dinocysts in the relative abundance (Fig. 2 D, E, and G).

The heterotrophic (H) and autotrophic (A) dinoflagellate cyst ratio (H/A) decreased during MIS 1 and 5e–5b, and presents higher values over the MIS 5a, 4 and 3. Oscillations in the H/A ratio were observed during the early MIS 3 (Fig. 2F).

4.3. Dinoflagellate cyst relative abundances

The autotrophic species (Figs. 2G and S3) were the most dominant during the interglacials MIS 5 and MIS 1. The most representative species during both interglacials were *Spiniferites bentorii* (up to 33%), *Spiniferites mirabilis* (up to 33%), *Spiniferites* spp. (up to 29%), *Spiniferites membranaceus* (up to 26%), and *Spiniferites pachydermus* (up to 26%). Other dominant autotrophic species were *Operculodinium centrocarpum* (up to 26%), *Tuberculodinium vancampoae* (up to 19%), *Pentapharsodinium dalei* (up to 18%) and *Impagidinium aculeatum* (up to 16%). The highest relative abundance of *Pentapharsodinium dalei* (~18–5%) occurred during MIS 5.

Leipokatium invisitatum is not common in the region and appears in a very low abundance. Despite that, *Leipokatium invisitatum* achieved values greater than 5% during the MIS 4 and was not excluded from the river outflow assemblage. The relative abundance of *Lingulodinium machaerophorum* reached a maximum of 31% during the early MIS 4. Cysts of heterotrophic taxa (Fig. S4) were the most common during MIS 3, mainly represented by *Brigantedinium* spp. (up to 66%), *Echinidinium*

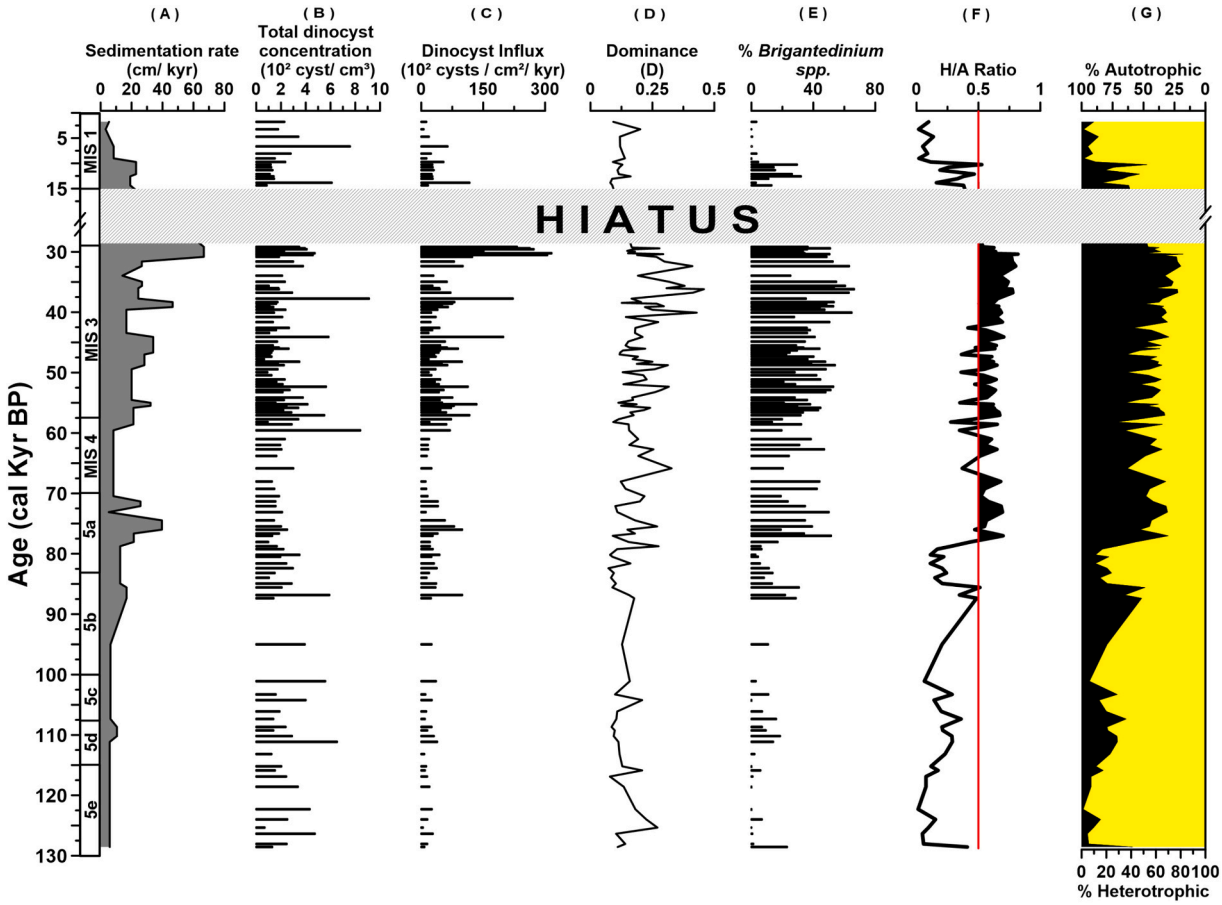

Fig. 2. A) Sedimentation rate (cm/kyr); B) Total dinocysts concentration (10^{2}cysts/cm^3); C) Dinocysts influx (10^{2}cysts/cm^2/kyr); D) Dominance index; E) Relative abundance of *Brigantedinium* spp.; F) H/A Ratio; G) Percentage of heterotrophic and autotrophic dinocysts with autotroph highlighted in yellow. (For interpretation of the references to colour in this figure legend, the reader is referred to the web version of this article.)

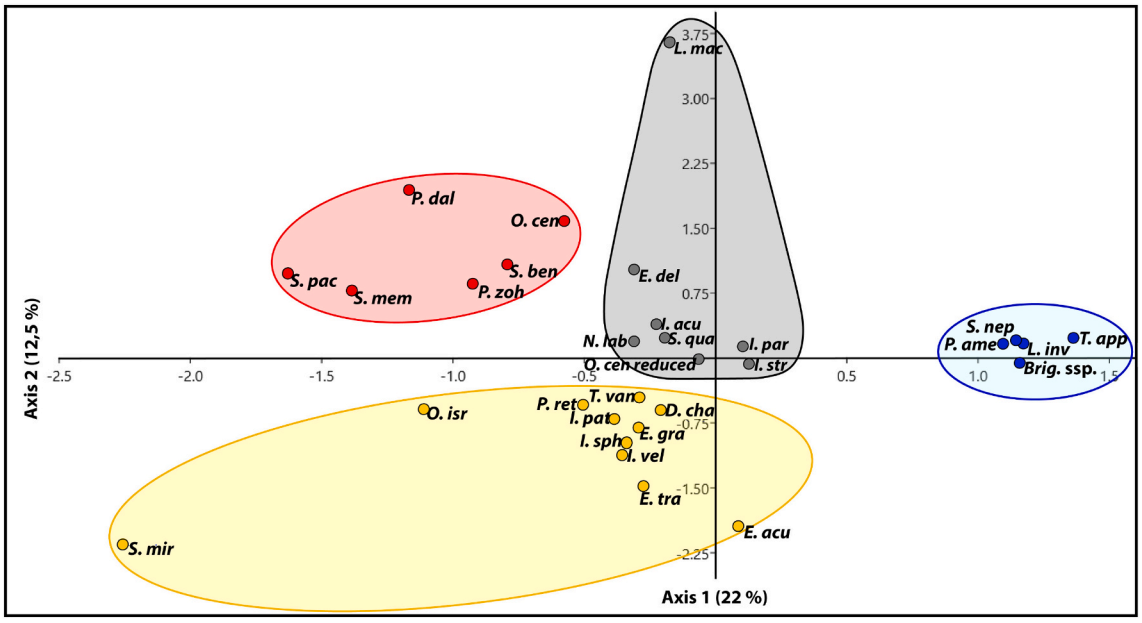

Fig. 3. The dinocysts Correspondence Analysis (CA) from the GL-1248 marine core, used to infer the ecological affinities. Four different assemblages were defined: 1- Open ocean assemblage was marked with red dots and composed by *Polysphaeridium- zoharyi* (*P. zoh*), *Pentapharsodinium dalei* (*P. dal*), *Operculodinium centrocarpum (O. cen), Spiniferites bentorii (S. ben), Spiniferites membranaceus (S. mem), Spiniferites pachydermus (S. pac);* 2- The neritic assemblage was marked with grey dots and established by *Echinidinium delicatum (E. del), Impagidinium aculeatum (I. acu), Impagidinium paradoxum (I. par), Impagidinium strialatum (I. str), Lingulodinium machaerophorum (L. mac), Nematosphaeropsis labyrinthus (N. lab), Operculodinium centrocarpum reduced processes (O. cen reduced), Selenopemphix quanta (S. qua);* 3- The river outflow assemblage was marked with blue dots and represented by *Brigantedinium* spp. *(Brig.* spp.*), Leipokatium invisitatum (L. Inv), Protoperidinium americanum (P. ame), Selenopemphix nephroides (S. nep), Trinovantedinium applanatum (T. app);* 4- The nutricline assemblage was marked with yellow dots and defined by *Dalella chathamensis (D. cha), Echinidinium aculeatum (E. acu), Echinidinium granulatum (E. gra), Echinidinium transparantum (E. tra), Impagidinium patulum (I. pat), Impagidinium sphaericum (I. sph), Impagidinium velorum (I. vel), Operculodinium israelianum (O. isr), Pyxidinopsis reticulata (P. ret), Spiniferites mirabilis (S. mir), Tuberculodinium vancampoae (T. van)*. (For interpretation of the references to colour in this figure legend, the reader is referred to the web version of this article.)

aculeatum (up to 34%), *Selenopemphix nephroides* (up to 23%), *Protoperidinium americanum* (up to 14%), *Trinovantedinium applanatum* (up to 11%), and *Selenopemphix quanta* (up to 8%).

4.4. Foraminifera relative abundances

We calculated the relative abundances of planktonic foraminifera over the last ~130 kyr. We use three species of planktonic foraminifera to assist the understanding of local hydrography and productivity. They were: *Globigerinoides ruber* (white, up to 47.5%), *Neogloboquadrina dutertrei* (up to 20%) and *Globigerinoides ruber* (pink, up to 11.8%) (Fig. S5).

5. Discussion

5.1. Dinoflagellate cysts ecological affinities

The CA established the ecological clusters between different dinoflagellate cysts (Fig. 3), which were in agreement with the literature. Arranged from values lower than −0.5 to the Axis 1 and higher than +0.5 values over the Axis 2, the following species were organized: *Polysphaeridium-zoharyi*, *Pentapharsodinium dalei*, *Operculodinium centrocarpum, Spiniferites bentorii, Spiniferites membranaceus, and Spiniferites pachydermus.* Those species are autotrophs and related to warm, oligotrophic, and more salinity waters (Vink et al., 2000; Kim et al., 2010; De Schepper et al., 2011). Due to the similarity with NBC features, we defined them as open ocean assemblage.

The *Brigantedinium* spp., *Protoperidinium americanum, Selenopemphix nephroides,* and *Trinovantedinium applanatum* are related to low-salinity and considered turbidity-tolerant species (Marret and Zonneveld, 2003; Kim et al., 2010). Both dinocysts *Selenopemphix nephroides* and *Trinovantedinium applanatum* were previously observed in the local area, associated with the Amazon River plume and characteristic of low-salinity and light-limited environments (Vink et al., 2000; Bouimetarhan et al., 2009; Bouimetarhan et al., 2018). The river outflow assemblage was highlighted by the positive values of the Axis 1, higher than 1, and established by the presence of *Brigantedinium* spp., *Leipokatium invisitatum, Protoperidinium americanum, Selenopemphix nephroides,* and *Trinovantedinium applanatum*.

In general, the species *Dalella chathamensis, Echinidinium aculeatum, Echinidinium granulatum, Echinidinium transparantum, Impagidinium patulum, Impagidinium sphaericum, Impagidinium velorum, Operculodinium israelianum, Pyxidinopsis reticulata, Spiniferites mirabilis, and Tuberculodinium vancampoae a*re related to well-ventilated water masses with higher nutrient availability as the South Atlantic Central Water (Vink et al., 2000; Zonneveld et al., 2013; Gu et al., 2017). We designated the assemblage of these species as nutricline, and they were disposed in values lower than +0.5 over the Axis 1 and in negative values of the Axis 2.

The neritic species are identified by their tolerance to transient features, as mixed water masses (Dale, 1996; Zonneveld and Brummer, 2000; Marret and Zonneveld, 2003). The neritic assemblage was defined by positive values of Axis 2 and ranging from 0.5 to −0.5 in Axis 1. The neritic assemblage was set up by *Echinidinium delicatum, Impagidinium, Impagidinium paradoxum, Impagidinium strialatum, Lingulodinium machaerophorum, Nematosphaeropsis labyrinthus, Operculodinium centrocarpum* reduced processes*, and Selenopemphix quanta.* Low salinity attenuates the *Operculodinium centrocarpum* process length (Ellegaard, 2000; Verleye et al., 2012), which corroborated with *Operculodinium centrocarpum* reduced processes included in the neritic assemblage. A complete list of species, ecological affinities, nutritional demands, selective preservation, and geographic distribution is shown in Table S1.

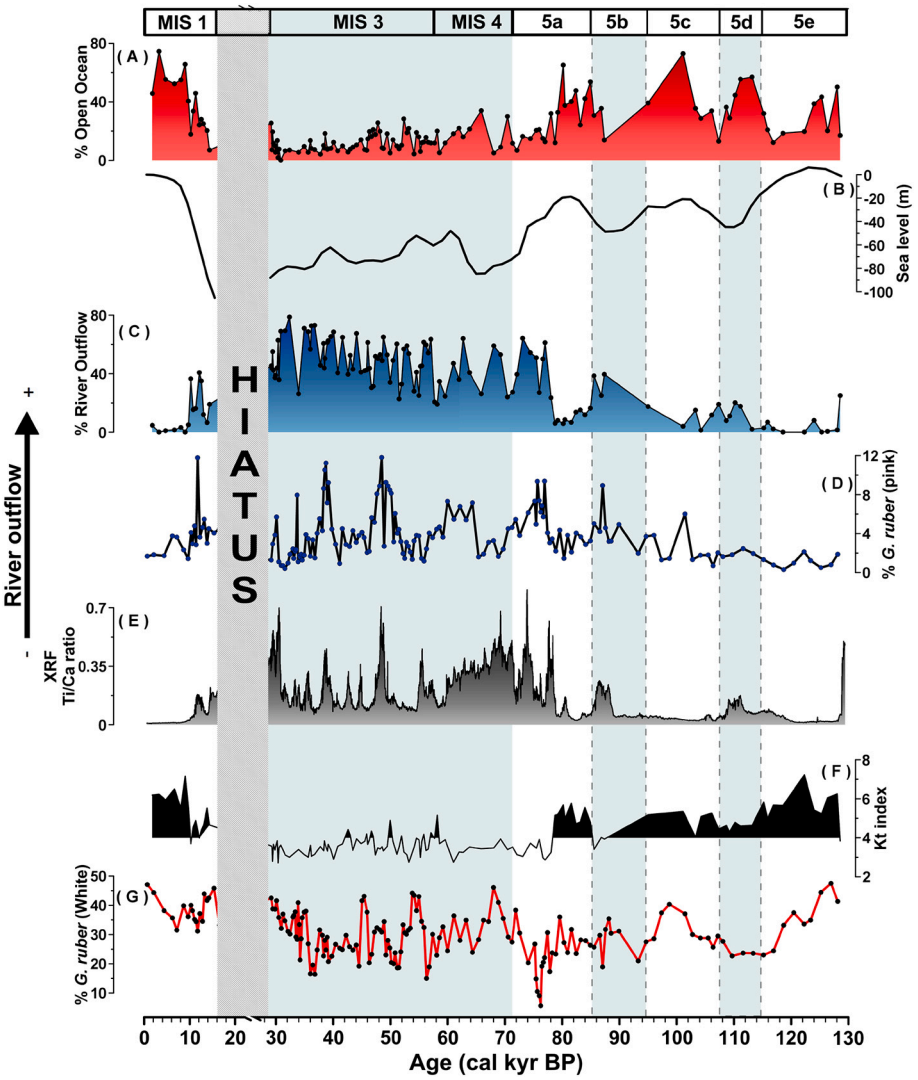

Fig. 4. Glacial-interglacial dinocyst assemblages pattern along with the last ~130 kyr. A) Open ocean assemblage relative abundance; B) Relative sea-level curve (Waelbroeck et al., 2002); C) River outflow assemblage relative abundance; D) *G. ruber* (pink) relative abundance; E) X-Ray fluorescence (XRF) Ti/Ca ratio (Venancio et al., 2018); F) kt index – S-cysts degradation index, with values higher than 4 filled in black; G) *G. ruber* (white) relative abundance. (For interpretation of the references to colour in this figure legend, the reader is referred to the web version of this article.)

5.2. Glacial-Interglacial changes of sea surface hydrography in the western equatorial Atlantic

Our results exhibited changes in the prevalence of dinocyst assemblages according to their nutritional requirements over the glacial and interglacial periods, as shown in Fig. 4. The open ocean assemblage showed a synchronous variation with RSL changes, with improved relative abundance during the interglacials (Fig. 4A and B). An opposite pattern was observed for the river outflow assemblage that increased in abundance during the entire glacial period when the RSL was lower compared to interglacials. We interpreted these patterns in the river outflow and open ocean assemblages as a consequence of glacial-interglacial changes in the RSL and fluvial contribution to the adjacent ocean. The proximity of the coastline to our core site enhanced the contribution of fluvial material, elevating turbidity, and dissolved inorganic nutrients supply in surface waters. Those changes, aligned with the reduced sea surface salinity (SSS), had a significant impact on phytoplankton response (Fig. 4B and C).

Another relevant aspect of the glacial period was the variability of precipitation over northeastern Brazil. High-latitude thermal changes with large intrusions of freshwater in the North Atlantic, known as Heinrich Stadials (HS), weakened the AMOC and reduced interhemispheric heat transport (Barker et al., 2009). The unbalanced distribution of sea surface temperatures over the Atlantic Ocean shifted the ITCZ towards the anomalously warm hemisphere (Broccoli et al., 2006; Mulitza et al., 2017). Consequently, northeastern Brazil experienced several wet phases due to the millennial-scale presence of the ITCZ to the south (Wang et al., 2004). The peaks in Ti/Ca ratio recorded in GL-1248 converge with the HS events and can be used as a tracer of fluvial discharge (Govin et al., 2012; Nace et al., 2014). The river outflow assemblage increased in abundance, due to their tolerance of low salinity waters and light limitation (Marret and Zonneveld, 2003; Richerol et al., 2008; Kim et al., 2010; Hardy et al., 2016). The presence of *G. ruber* (*pink*) corroborated Ti/Ca fluctuations due to its affinity for low SSS and warm waters, and imprints better response to the precipitation events than to the RSL changes or the increase of turbidity at the sea surface (Schmuker and Schiebel, 2002).

Although the glacial boundary conditions acted in favor of river outflow assemblage, we investigated the preservation of the dinocysts using the kt index (Zonneveld et al., 2010) (Fig. 4F). The kt index exhibited values higher than 4 during interglacials, which suggested that the degradation of S-cysts needs to be taken into consideration due to

more oxygenated waters at the surface sediments (Zonneveld et al., 2010). Thus, the response of the river outflow assemblage may be underestimated during the interglacials, since almost half of the river outflow species (*Brigantedinium* spp. and the *P. americanum*) are sensitive to oxidative waters as shown in Table S1. Notwithstanding, the low relative abundance of the river outflow assemblage (< 20%) was consistent with the decrease in river freshwater input during interglacials and was corroborated by reduced relative abundances of *G. ruber* (pink) (< 4%) and Ti/Ca ratio values (< 0.2) (Fig. 4C, D, and E). Compared to the glacial period, the RLS was higher in interglacials and may have hampered the influence of fluvial waters on the GL-1248 sediment core site.

Over the interglacial periods, the RSL was higher, and the coastal contribution was narrowed. The open ocean assemblage prevailed over the interglacial periods, and this assemblage is composed of autotrophs dinocysts with low demand for nutrients (Vink et al., 2000; Bouimetarhan et al., 2009). We also applied the *G.ruber* (white) relative abundance as an indicator of warm and oligotrophic conditions in the water column (Kucera, 2007). Changes in the *G.ruber* (white) values were consistent with the general trend of the open ocean assemblage over the interglacials. During the glacial period, both proxies didn't correlate, as the *G. ruber* (white) relative abundance didn't show a pattern similar to the oscillation of RSL (Fig. 4G, A and B), and probably varied according to changes in sea surface temperature (SST).

5.3. Oscillations of autotrophic assemblages over interglacials

The relative abundance of open ocean assemblage and *G. ruber* (white) transpassed 35% during the MIS 1 and over most of the warm intervals of MIS 5 (Fig. 5A and B). Despite divergences over the MIS 5d, both proxies indicated the prevalence of warm, saline, and oligotrophic tropical waters at the sea surface during the interglacials. In contrast, the predominant assemblages of dinocysts presented an intermittent behavior and oscillated between open ocean and nutricline over the MIS5. Autotrophs dinocysts denoted the same nutritional strategy. Still, the nutricline and open ocean assemblages differed by their requirements of nutrient concentration (see Table S1). It is noteworthy that the nutricline assemblage improved its relative abundance (> 60%) during the warm substage MIS 5e (Fig. 5C) with particular highlight to the specie *S. mirabilis* (Fig. S3). The asynchrony between nutricline and the open ocean assemblage indicated oscillations in the concentration of the nutrients in the water column. The high RLS characteristic of interglacials followed by low Ti/Ca values (< 0.2), used as a proxy of the continental source (Fig. 5D), led us to consider a different source of nutrients. Thus, these nutrients might come from more enriched water masses such as the SACW located below the thermocline. Other local studies also suggested more availability of nutrients during the warm substages of MIS 5 (Rühlemann et al., 1996; Mulitza et al., 1998; Vink et al., 2002).

The MIS 5e was considered an analog to pre-industrial temperature with similar atmospheric CO_2 concentration, but with distinct orbital conditions and reduced north pole ice cap coverage (Dutton et al., 2015). Venancio et al. (2018) showed changes in upper ocean stratification in high-resolution for the record of GL-1248 marine sediment core. A thermal stratification index was constructed based on planktonic foraminifera with distinct ecological distribution in the water column and applied to reconstruct variations on the thermocline depth according to the trade wind system. We suggested that the discrepancies in orbital eccentricity and insolation between MIS 5e and MIS1 (Fig. 6E and F) led to differences in trade winds system intensity. Possibly the decrease of the meridional temperature gradient over the Atlantic Ocean during the warm substages of the last interglacial may have provoked less intense trade winds over the equatorial Atlantic Ocean. Weakened zonal winds potentially attenuated the accumulation of warm surface waters in western equatorial Atlantic, enabling the intrusion of SACW nutrients in the photic zone. The minimal stratification corroborated with our suggestion of enhanced availability of nutrients over the MIS 5e when compared with MIS 1 (Fig. 5G). Another evidence for the relevance of trade winds to reduced stratification of thermocline at the western equatorial Atlantic during the warm periods of MIS 5 interglacials was the in-phase response of GL-1248 nutricline assemblage with the *F. profunda* high abundance in the RC24-7 marine sediment core (1′20.5′S, 11′53.3′W), a coccolithophorid species associated with a deep nutricline at the eastern equatorial Atlantic (Molfino and McIntyre, 1990). Both proxies indicate that SE trade winds and SEC transport were reduced during the perihelion in June, boreal summer. Reduced transport of warm waters to the western portion of the equatorial Atlantic, consequently attenuated the piled up of water masses and triggered the proposed mechanisms. Vink et al. (2002) had already suggested weak trade winds as a possible mechanism that led to a shallower thermocline in the western equatorial Atlantic region.

5.4. Millennial-scale changes in productivity in the western equatorial Atlantic

The river outflow assemblage showed millennial-scale changes through the last glacial. The increase in the relative abundance of river outflow assemblage was linked to changes in the relative abundance of *Brigantedinium* spp. Between 65 and 30 kyr, the observed changes in river outflow assemblage seemed to match with HS4, HS5, HS5A (Fig. 6A and B). The input of freshwaters by continental contribution increased during the last glacial with maxima during HS millennial-scale events (Govin et al., 2012; Nace et al., 2014). The study of Zhang et al. (2015) using neodymium (Nd) isotopic compositions of marine sediment cores GeoB 16,224–1 and GeoB 16,206–1 showed no significant Amazon river contribution to our study area during HS1 (period of reduced AMOC transport). Based on these findings, we assume that the Parnaiba river was the main continental source during HS events.

Despite the match between the river outflow assemblage and HS events, no significant improvement was observed during the HS6 and HS3. The river outflow assemblage displayed a gradual decrease within the event during late MIS4, similar to the Ti/Ca ratio (Fig. 6A and B), indicating a fluvial sediment retrenchment. In the continental part, the vegetation reflects the precipitation pattern. The millennial-scale precipitation events in northeastern Brazil was possibly the main driver of changes in vegetation structure. The increment of vegetation in the vicinity of the Parnaiba hydrographic basin might have promoted the soil stability, reducing the weathering (Dupont et al., 2010; Bouimetarhan et al., 2018). Prolonged wet periods probably induced the growth of trees and shrubs, which might have reduced the suspended material in the river plume. Low salinity sea surface and more light penetration benefit the widespread of neritic species (Fig. 6C), as the pronounced increase of *Lingulodinium machaerophorum* (Fig. S3) by the end of H6 indicated. For HS3, although there was a high relative abundance of river outflow assemblage (~80–70%) within the event, it was not synchronous with major Ti/Ca fluctuations. The mismatch of results is not clear. Still, we suggest that it may have occurred due to competition between species of the river outflow and nutricline assemblages, as a consequence of the low sea level over the shallow continental shelf, harming the dominance of the river outflow assemblage (Fig. 6B and E).

Modern ecological studies show that the phytoplankton size-structure might change due to variations in the nutrient source, increasing the grazing (Cuevas et al., 2019). A robust input of freshwater in the adjacent ocean was possibly coupled with large amounts of dissolved inorganic nutrients, and enhanced turbulence at the sea surface creates perfect conditions to improve the primary productivity by diatoms (Smayda and Reynolds, 2001). Heterotrophs dinoflagellates are diatoms' predators and can be interpreted as an indirect primary productivity proxy. The pronounced increase of heterotrophs dinocysts

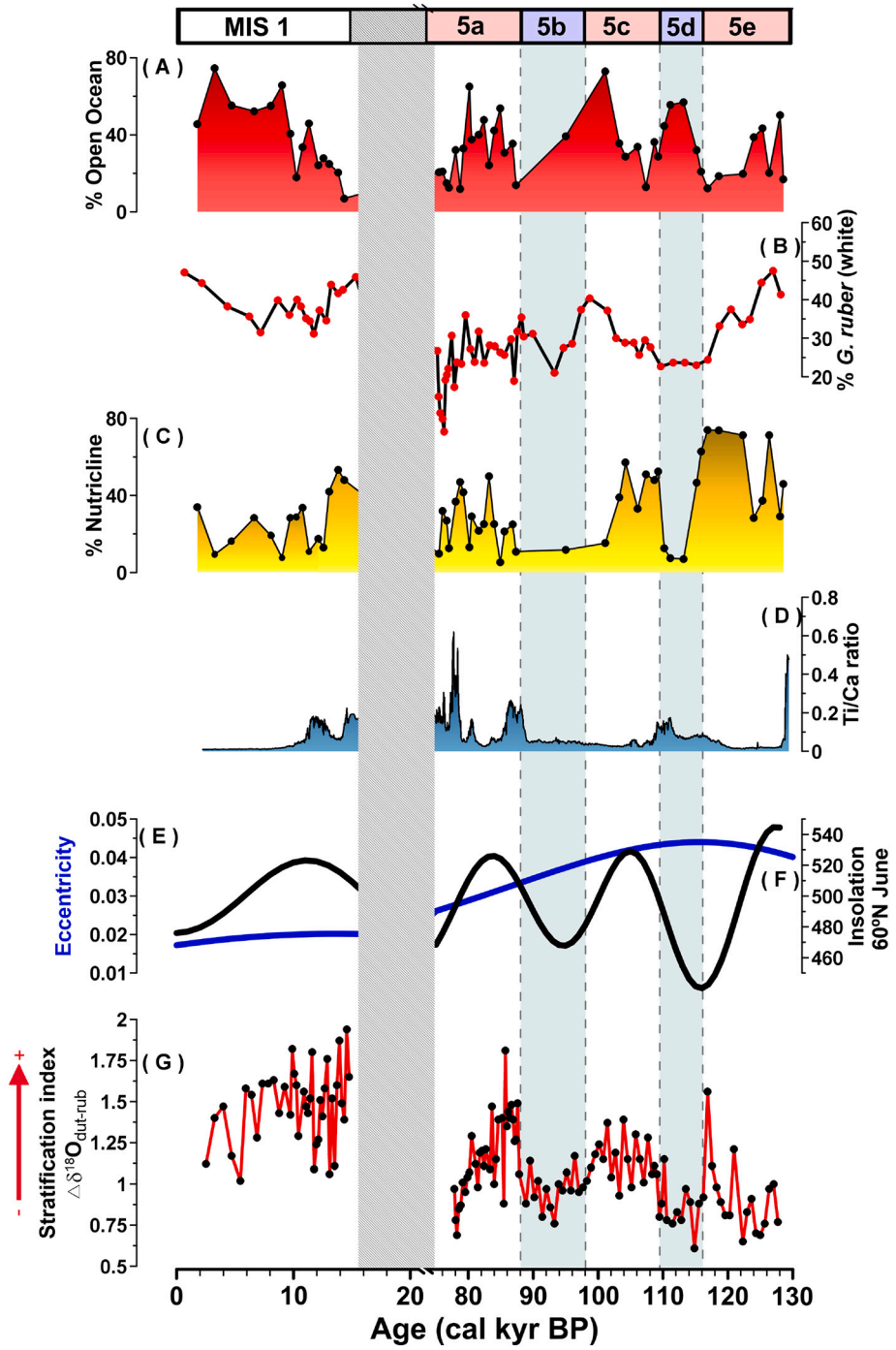

Fig. 5. Comparisons between interglacials. A) The relative abundance of open ocean assemblage; B) The relative abundance of *G. ruber* (white); C) The relative abundance of nutricline assemblage; D) XRF Ti/Ca ratio (Venancio et al., 2018); E) Orbital eccentricity oscillation; F) Insolation of June at 60°N (Berger and Loutre, 1991); G) Stratification index $\Delta\delta^{18}O_{dut\text{-}rub}$ (Venancio et al., 2018).

over the glacial was given by the combination of more tolerance to low salinity water and light restriction. Still, another possible factor that possibly enabled food for heterotrophic dinocysts was the shift in the phytoplankton community (Jeong et al., 2004).

Even in the absence of diatoms information for the record, we may not assume low productivity over the glacial period. The specie *N. dutertrei* is endemic of the western equatorial Atlantic, known as a tracer of higher productivity, and already used to infer the vertical mixing over the glacial period (Cléroux et al., 2013; Portilho-Ramos et al., 2017). The *N. dutertrei* feed on phytoplankton without preferences and can be viewed as an intermediate indicator between the response of the river outflow and nutricline assemblage. Despite that, other environmental features beyond productivity could be imprinted in *N. dutertrei* response, such as temperature changes and open ocean conditions. The mechanisms leading the nutricline assemblage pattern over the glacial were not evident, and changes in the relative abundances of *N. dutertrei* didn't follow the same trend of the nutricline assemblage (Fig. 6D and E).

Despite the predominance of heterotrophic dinocysts during the glacial, the H/A ratio oscillates in the early MIS 3 (~60–45 kyr BP). The H/A ratio fluctuation indicates changes in the nutrient source in millennial-scale variability. The reductions in the nutricline assemblage

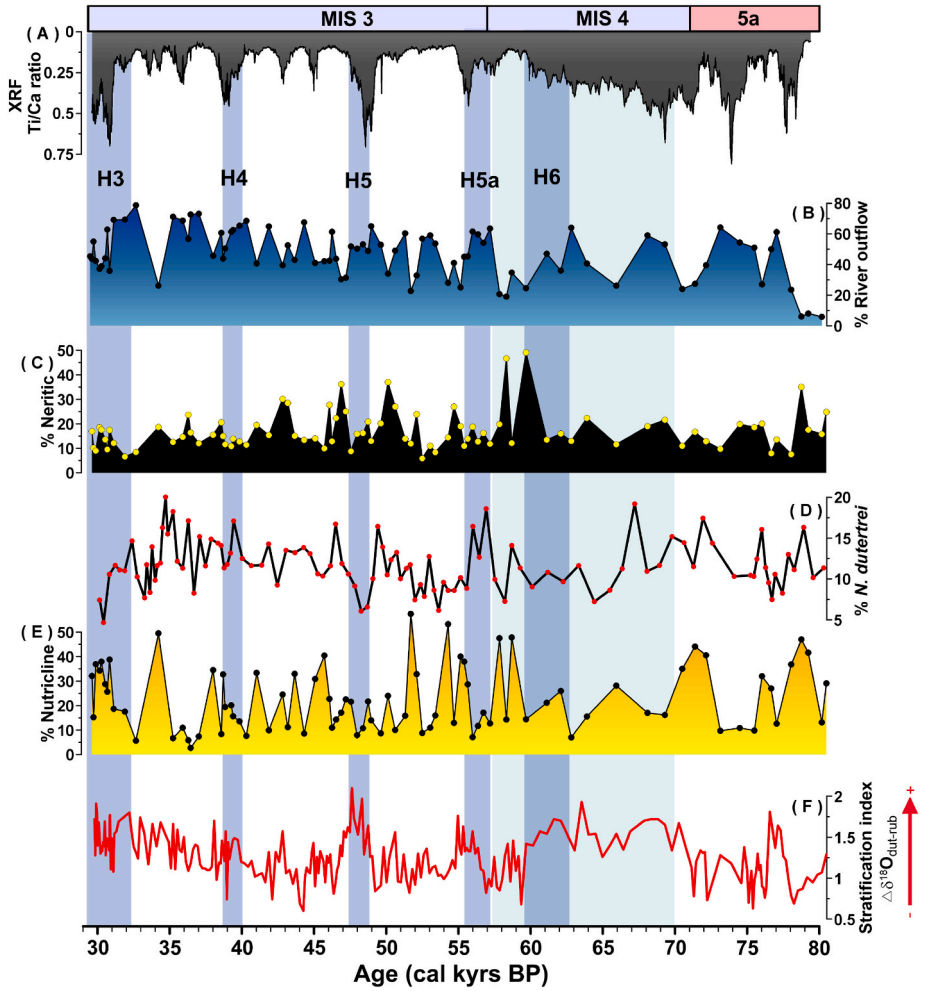

Fig. 6. Millennial-scale variations in dinocyst assemblages between MIS 5a and MIS 3. A) XRF Ti/Ca ratio (Venancio et al., 2018); B) Relative abundance of the river outflow assemblage; C) Relative abundance of the neritic assemblage; D) Relative abundance of *N. dutertrei*; E) Relative abundance of the nutricline assemblage; F) Stratification index $\Delta\delta^{18}O_{dut\text{-}rub}$ (Venancio et al., 2018).

during HS, except HS3, suggest that dinoflagellate productivity was low during these events. In contrast, the nutricline assemblage had improved its relative abundance (> 30%) post-HS events (H6, H5a, and H4). In the western equatorial South Atlantic, the SE trade winds modulate the transport of the SEC and the NBC (Johns et al., 1998; Stramma et al., 1995), and during HS events the AMOC is reduced, as well as the transport of SEC and NBC (McManus et al., 2004). Portilho-Ramos et al. (2017) demonstrated that the ITCZ displacements promoted more wind-driven vertical mixing near NE Brazil and deepened the mixed layer. Aligned with that, the stratification index values oscillated between 0.75 and 2.0 over the glacial period, with reduced stratification values before and after HS events (Venancio et al., 2018). The peaks in the relative abundance of the nutricline assemblage might be explained by the conjuncture of factors, as the reduced river discharge, more wind-driven vertical mixing post-HS events, and with the relaxation of the thermal stratification of the thermocline (Fig. 6F). The reestablishment of NBC promoted by more vigorous SE trade winds increased the mix-wind and provided more nutrients in the photic zone. In general, our proxies pointed to a more productive glacial period than previously considered for the region (Rühlemann et al., 1996; Bickert et al., 1997; Mulitza et al., 1998).

6. Conclusions

We investigated the hydrography and productivity changes in an oligotroph region over distinct past climatic backgrounds. The dinocyst assemblages showed to be sensitive to different nutrient sources and ocean-atmosphere processes. The autotrophic taxa prevailed during the interglacials, and heterotrophic taxa were more abundant over the glacial period. Singularities in dinoflagellate assemblages were observed between interglacial periods (Holocene and MIS 5e). The particular orbital features of each interglacial period created different thermal gradients throughout the Atlantic ocean and altered the trade winds' intensity between them. Two autotrophic dinocyst assemblages with distinct nutrient requirements (open ocean and nutricline) interchanged the predominance over the Holocene and MIS 5e. The antiphase between the open ocean and nutricline assemblages denoted mainly fluctuations in the availability of nutrients in the photic zone. The significant increase in the relative abundance of nutricline assemblage during the MIS 5e suggested a more productive period than MIS1. Attenuated trade winds during MIS 5e might have promoted the relaxation of thermocline stratification at western equatorial Atlantic, facilitating nutrient diffusion in the photic zone.

During the last glacial period, the enhanced gradient of temperature over the Atlantic ocean compressed climatic zones towards the equator, driving more vigorous trade winds. The displacements of ITCZ were accompanied by the reduction of Parnaíba river discharge and the intensification of SE trade winds, which enabled the northward transport of warmer sea surface waters. The strengthened of SE trade winds promoted enhanced wind-driven vertical mixing in the ocean surface

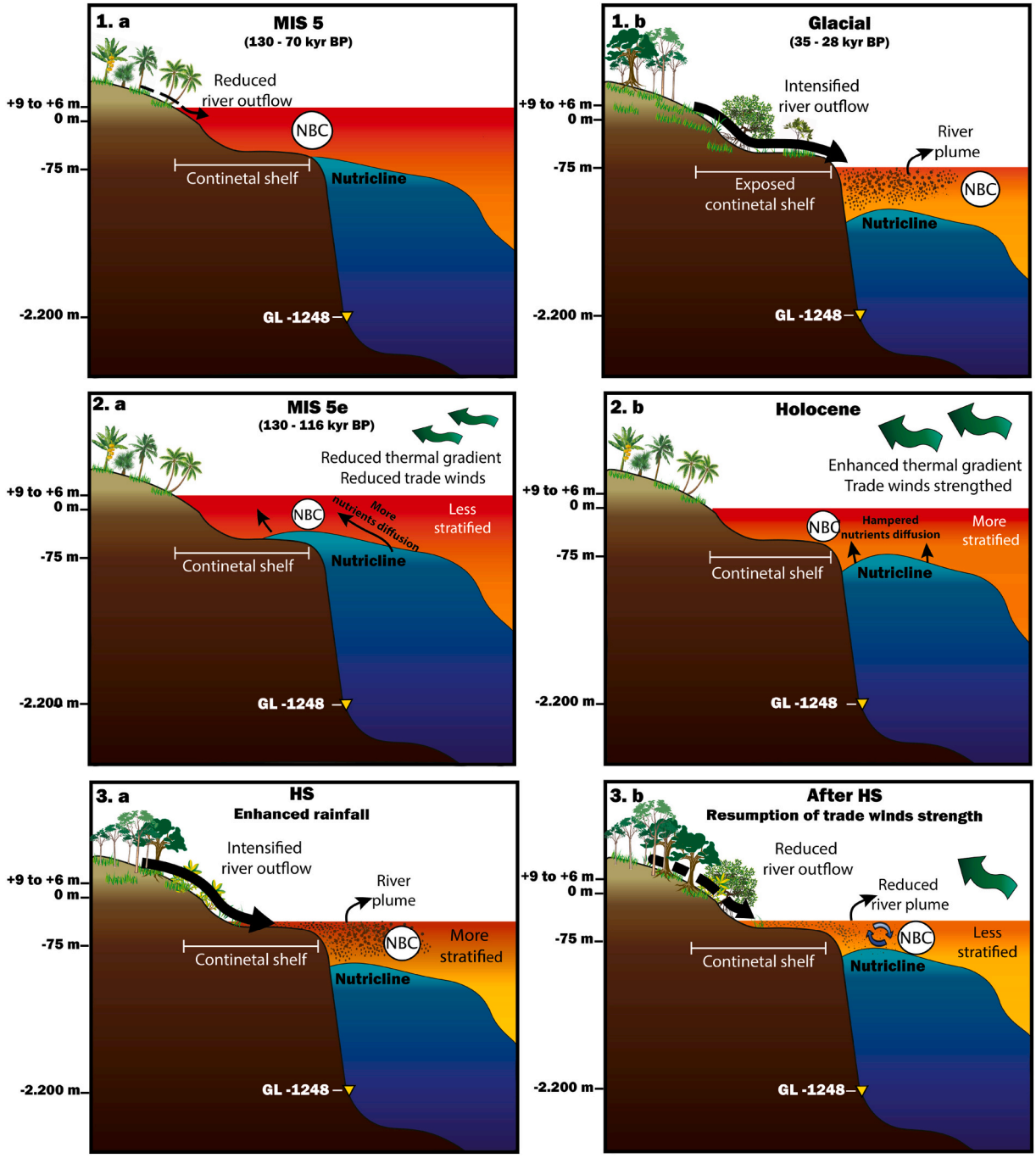

Fig. 7. The conceptual model with the main environmental forces acting on three different scenarios: 1) Comparisons between MIS 5 and the last glacial hydrography, with sea-level and continental contribution discrepancies, and the NBC proximity to the continental shelf; 2) Comparisons between interglacials, with singular differences in trade winds intensity and nutrient diffusion in the photic zone; 3) Comparisons between HS and post-HS, with changes in river outflow, river plume, vegetation, and trade winds intensity. The blue arrows indicate the vertical mixing occurring in the water column. The size of the arrows is a reference to the quantity of the proposed processes. The gradient of colors in the ocean (red to orange), also represents the thermal stratification. (For interpretation of the references to colour in this figure legend, the reader is referred to the web version of this article.)

and a shallower thermocline, indicated by low values of the stratification index (< 1). The ITCZ shifts probably improved the relative abundance of nutricline assemblage post-HS events, as more nutrients were available in the photic zone. The HS events were marked by the prolonged presence of the ITCZ over northeastern Brazil, and followed by a substantial fluvial input to the adjacent ocean. The intensified runoff might have increased the turbidity and turbulence on the sea surface. We suggest that the autotrophic phytoplankton community shifted preferentially from dinoflagellates to diatoms. Still, the heterotrophic dinocysts were benefited over the glacial period by the presence of diatoms, increased turbidity, and low salinity. The pronounced wet periods might have altered the structure of continental vegetation, with more trees and shrubs. The enhanced soil stability possibly reduced the river plume turbidity and benefited the neritic assemblage by the end of HS6. We created conceptual models of environmental processes during past intervals, as previously described in our discussions (Fig. 7).

Declaration of Competing Interest

The authors declare that they have no known competing financial interests or personal relationships that could have appeared to influence the work reported in this paper.

Acknowledgments

We thank R. Kowsman (CENPES/Petrobras) and Petrobras Core Repository staff (Macaé/Petrobras) for providing sediment core GL-1248. The financial support for this study is given to the first author from the Brazil National Council for the Improvement of Higher Education (CAPES). CAPES also financially supported Patricia S. Piacsek Borges with a scholarship from the CAPES-ASPECTO project (Grant 88887.091731/ 2014-01). Fang Gu is thanked for the support of dinocyst identification. CAPES financially supported I. M. V. with a scholarship (grant 88887.156152/2017-00 and 88881.161151/2017-01). This study was financed by the CNPq Project RAiN (grant 406322/2018-0).

Appendix A. Supplementary data

Supplementary data to this article can be found online at https://doi.org/10.1016/j.palaeo.2020.109952.

References

Barker, S., Diz, P., Vautravers, M.J., Pike, J., Knorr, G., Hall, I.R., Broecker, W.S., 2009. Interhemispheric Atlantic seesaw response during the last deglaciation. Nature 457 (7233), 1097.
Benninghoff, W.S., 1962. Calculation of pollen and spores density in sediments by the addition of exotic pollen in known quantities. Pollen Spores 4 (2), 332–333.
Berger, A., Loutre, M.-F., 1991. Insolation values for the climate of the last 10 million of years. Quat. Sci. Rev. 10 (4), 297–317.
Bickert, T., Curry, W.B., Wefer, G., 1997. Late Pliocene to Holocene (2.6–0 Ma) western equatorial Atlantic deep-water circulation: Inferences from benthic stable isotopes. In: Ocean Drilling Program. 154. pp. 239–254.
Blaauw, M., 2010. Methods and code for 'classical' age-modeling of radiocarbon sequences. Quat. Geochronol. 5 (5), 12–518.
Bouimetarhan, I., Marret, F., Dupont, L., Zonneveld, K., 2009. Dinoflagellate cyst distribution in marine surface sediments off West Africa (17-6°N) in relation to sea-surface conditions, freshwater input and seasonal coastal upwelling. Mar. Micropaleontol. 71, 113–130.
Bouimetarhan, I., Chiessi, C.M., Gonzalez-Arango, C., Dupont, L., Voigt, I., Prange, M., Zonneveld, K., 2018. Intermittent development of forest corridors in northeastern Brazil during the last deglaciation: Climatic and ecologic evidence. Quat. Sci. Rev. 192, 86–96.
Broccoli, A.J., Dahl, K.A., Stouffer, R.J., 2006. Response of the ITCZ to Northern Hemisphere cooling. Geophys. Res. Lett. 33 (L01702).
Cléroux, C., deMenocal, P., Arbuszewski, J., Linsley, B., 2013. Reconstructing the upper water column thermal structure in the Atlantic Ocean. Paleoceanography 28, 503–516.
Cuevas, L.A., Tapia, F.J., Iriarte, J.L., González, H.E., Silva, N., Vargas, C.A., 2019. The interplay between freshwater discharge and oceanic waters modulates phytoplankton size-structure in fjords and channel systems of the Chilean Patagonia. Prog. Oceanogr. 173, 103–113.
Dale, B., 1996. Dinoflagellate cyst ecology: Modeling and geological applications. In: Jansonius, J., McGregor, D.G. (Eds.), Palynology: Principles and Applications, third ed. American Association of Stratigraphic Palynologists, Salt Lake City, UT, pp. 1249–1275.
De Schepper, S., Fischer, E.I., Groeneveld, J., Head, M.J., Matthiessen, J., 2011. Deciphering the palaeoecology of late Pliocene and early Pleistocene dinoflagellate cysts. Palaeogeogr. Palaeoclimatol. Palaeoecol. 309, 17–32.
Dupont, L.M., Schlütz, F., Ewah, C.T., Jennerjahn, T.C., Paul, A., Behling, H., 2010. Two-step vegetation response to enhanced precipitation in Northeast Brazil during Heinrich event 1. Glob. Chang. Biol. 16, 1647–1660.
Dutton, A., Carlson, A.E., Long, A.J., Milne, G.A., Clark, P.U., Deconto, R., Horton, B.P., Rahmstorf, S., Raymo, M., 2015. Sea-level rise due to polar ice-sheet mass loss during past warm periods. Science 349, 153.
Ellegaard, M., 2000. Variations in dinoflagellate cyst morphology under conditions of changing salinity during the last 2000 years in the Limfjord, Denmark. Rev. Palaeobot. Palynol. 109 (1), 65–81.
Faegri, K., Iversen, J., 1989. In: Faegri, K., Kyrland, P.E., Krzywinski, K. (Eds.), Textbook of Pollen Analysis, 4th ed. John Wiley and Sons, Chichester (328 pp).
Gaines, G., Elbrächter, M., 1987. Heterotrophic nutrition. In: Taylor, F.J.R. (Ed.), The Biology of Dinoflagellates. Blackwell, Oxford, pp. 224–268.
Govin, A., Holzwarth, U., Heslop, D., Ford Keeling, L., Zabel, M., Mulitza, S., Collins, J.A., Chiessi, C.M., 2012. Distribution of major elements in Atlantic surface sediments (36°N-49°S): Imprint of terrigenous input and continental weathering. Geochem. Geophys. Geosyst. 13, 1–23.
Gu, F., Zonneveld, K.A.F., Chiessi, C.M., Arz, H.W., Jürgen, P., Behling, H., 2017. Long-term vegetation, climate and ocean dynamics inferred from a 73, 500 years old marine sediment core (GeoB2107-3) off southern Brazil. Quat. Sci. Rev. 172, 55–71.
Hammer, Ø., Harper, D.A.T., Ryan, P.D., 2001. PAST: Paleontological Statistics Software Packyrge for Education and Data Analysis. Palaeontol. Electron. 4, 9.
Hardy, W., Penaud, A., Marret, F., Bayon, G., Marsset, T., Droz, L., 2016. Dinocyst assemblage constraints on oceanographic and atmospheric processes in the eastern equatorial Atlantic over the last 44 kyr. Biogeosciences 13, 4823–4841.
Hastenrath, S., 2012. Exploring the climate problems of Brazil's Nordeste: a review. Clim. Chang. 112 (2), 243–251.
Hastenrath, S., Merle, J., 1987. The annual cycle of subsurface thermal structure in the tropical Atlantic Ocean. J. Phys. Oceanogr. 17, 1518–1538.
Herbland, A., Voituriez, B., 1979. Hydrological structure analysis for estimating the primary production in the tropical Atlantic Ocean. J. Mar. Res. 37 (1), 87–101.
Jeong, H.J., Yoo, Y.D., Kim, S.T., Kang, N.S., 2004. Feeding by the heterotrophic dinoflagellate Protoperidinium bipes on the diatom Skeletonema costatum. Aquat. Microb. Ecol. 36, 171–179.
Johns, W.E., Lee, T.N., Beardsley, R.C., Candela, J., Limeburner, R., Castro, B., 1998. Annual cycle and variability of the North Brazil current. J. Phys. Oceanogr. 28, 103–128.
Jongman, R.H.G., ter Braak, C.J.F., van Tongeren, O.F.R., 1987. Data Analysis in Community and Landscape Ecology. Pudoc, Wageningen. (299 pp).
Kennett, J.P., Srinivasan, M.S., 1983. Neogene Planktonic Foraminifera: A Phylogenetic Atlas. Hutchinson Ross, Stroudsburg, Pennsylvania (265 pp).
Kim, S., Scourse, J., Marret, F., Lim, D., 2010. A 26,000-year integrated record of marine and terrestrial environmental change off Gabon, west equatorial Africa. Palaeogeogr. Palaeoclimatol. Palaeoecol. 297, 428–438.
Kinkel, H., Baumann, K.-H., Čepek, M., 2000. Coccolithophores in the equatorial Atlantic Ocean: response to seasonal and Late Quaternary surface water variability. Mar. Micropaleontol. 39, 87–112.
Krauss, W., 1996. The warm water sphere of the North Atlantic Ocean. Gebruder Borntraeger 466.
Krueger, A., Murphy, M., Gilbert, E., Burke, K., 2012. Deposition and deformation in the deepwater sediment of the offshore Barreirinhas Basin, Brazil. Geosphere 1–26.
Kucera, M., 2007. Planktonic foraminifera as tracers of past oceanic environments. In: Hillaire-Marcel, C., de Vernal, A. (Eds.), Developments in Marine Geology: Proxies in Late Cenozoic Paleoceanography. Elsevier, Montreal, pp. 213–262.
Legendre, P., Gallagher, E.D., 2001. Ecologically meaningful transformations for ordination of species data. Oecologia 129, 271–280.
Leroux, M., 1993. The Mobile Polar High: a new concept explaining present mechanisms of meridional air-mass and energy exchanges and global propagation of paleoclimatic changes. Glob. Planet. Chang. 7, 69–93.
Lisiecki, L.E., Raymo, M.E., 2005. A Pliocene-Pleistocene stack of 57 globally distributed benthic δ18O records. Paleoceanography 20 (PA1003).
Loeblich, A., Tappan, H., 1988. Foraminiferal Genera and their Classification. Van Nostrand Reinhold Company, New Yourk (970 pp).
Mallin, M.A., Paerl, H.W., Rudek, J., Bates, P.W., 1993. Regulation of estuarine primary production by watershed rainfall and river flow. Mar. Ecol. Prog. 93, 199–203.
Marret, F., Zonneveld, K.A.F., 2003. Atlas of modern organic-walled dinoflagellate cyst distribution. Rev. Palaeobot. Palynol. 125, 1–200.
McManus, J.F., Francois, R., Gherardi, J.-M., Keigwin, L.D., Brown-Leger, S., 2004. Collapse and rapid resumption of Atlantic meridional circulation linked to deglacial climate changes. Nature 428, 834–837.
Mohriak, W.U., 2003. In: Bizzi, L.A., Schobbenhaus, C., Gonçalves, R.M.V. (Eds.), Sedimentary Basins of the Brazilian Continental Margin. Geologia, Tectônica e Recursos Minerais Do Brasil, Texto, Mapas & SIG, Brasília, pp. 87–94.
Molfino, B., McIntyre, A., 1990. Precessional forcing of nutricline dynamics in the equatorial Atlantic. Science 249, 766–769.
Molinari, R.L., Garzoli, S.L., Katz, E.J., Harrison, D.E., Richardson, P.L., Reverdin, G., 1986. A synthesis of the First GARP Global Experiment (FGGE) in the equatorial Atlantic Ocean. Prog. Oceanogr. 16, 91–112.
Mulitza, S., Rühlemann, C., Bickert, T., Hale, W., 1998. Late Quaternary δ13C gradients and carbonate accumulation in the western equatorial Atlantic. Earth Planet. Sci. Lett. 155, 237–249.
Mulitza, S., Chiessi, C.M., Schefuß, E., Lippold, J., Wichmann, D., Antz, B., Mackensen, A., Paul, A., Prange, M., Rehfeld, K., Werner, M., Bickert, T., Frank, N., Kuhnert, H., Lynch-Stieglitz, J., Portilho-Ramos, R.C., Sawakuchi, A.O., Schulz, M., Schwenk, T., Tiedemann, R., Vahlenkyrmp, M., Zhang, Y., 2017. Synchronous and proportional deglacial changes in Atlantic meridional overturning and northeast Brazilian precipitation. Paleoceanography 32 (6), 622–633.
Nace, T.E., Baker, P.A., Dwyer, G.S., Silva, C.G., Rigsby, C.A., Burns, S.J., Giosan, L., Otto-Bliesner, B., Liu, Z., Zhu, J., 2014. The role of North Brazil Current transport in the paleoclimate of the Brazilian Nordeste margin and paleoceanography of the western tropical Atlantic during the late Quaternary. Palaeogeogr. Palaeoclimatol. Palaeoecol. 415, 3–13.
Parkin, D.W., 1974. Trade-winds during the glacial cycles. Proc. R. Soc. Lond. A 337, 73–100.
Peterson, R.G., Stramma, L., 1991. Upper-level circulation in the South Atlantic. Prog. Oceanogr. 26, 1–73.
Portilho-Ramos, R.C., Chiessi, C.M., Zhang, Y., Mu, S., Kucera, M., Siccha, M., Prange, M., Paul, A., 2017. Coupling of equatorial Atlantic surface stratification to glacial shifts in the tropical rain belt. Nat. Sci. Rep. 1561, 1–8.
Pospelova, V., Kim, S.-J., 2010. Dinoflagellate cysts in recent estuarine sediments from

aquaculture sites of southern South Korea. Mar. Micropaleontol. 76, 37–51.
Price, A.M., Pospelova, V., Coffin, M.R.S., Latimer, J.S., Chmura, G.L., 2016. Biogeography of dinoflagellate cysts in Northwest Atlantic estuaries. Ecol. Evol. 6 (16), 5648–5662.
Reimer, P.J., Bard, E., Bayliss, A., Beck, J.W., Blackwell, P.G., Ramsey, C.B., Buck, C.E., Cheng, H., Edwards, R.L., Friedrich, M., Grootes, P.M., Guilderson, T.P., Haflidason, H., Hajdas, I., Hatté, C., Heaton, T.J., Hoffmann, D.L., Hogg, A.G., Hughen, K.A., Kaiser, K.F., Kromer, B., Manning, S.W., Niu, M., Reimer, R.W., Richards, D.A., Scott, E.M., Southon, J.R., Staff, R.A, Turney, C.S.M., van der Plicht, J., 2013. IntCal13 and Marine13 radiocarbon age calibration curves 0–50,000 years cal BP. Radiocarbon 55 (04), 1869–1887.
Richerol, T., Rochon, A., Blasco, S., Scott, D.B., Schell, T.M., Bennett, R.J., 2008. Distribution of dinoflagellate cysts in surface sediments of the Mackenzie Shelf and Amundsen Gulf, Beaufort Sea (Canada). J. Mar. Res. 74, 825–839.
Rühlemann, C., Frank, M., Hale, W., Mangini, A., Mulitza, S., Muller, P.J., Wefer, G., 1996. Late Quaternary productivity changes in the western equatorial Atlantic: evidence from 230Th-normalized carbonate and organic carbon accumulation rates. Mar. Geol. 135 (1–4), 127–152.
Schmuker, B., Schiebel, R., 2002. Planktic foraminifers and hydrography of the eastern and northern Caribbean Sea. Mar. Micropaleontol. 46 (3–4), 387–403.
Schott, F.A., Stramma, L., Fischer, J., 1995. The warm water inflow into the western tropical Atlantic boundary regime, spring 1994. J. Geophys. Res. 100, 24745–24760.
Smayda, T.J., Reynolds, C.S., 2001. Community assembly in marine phytoplankton: Application of recent models to harmful dinoflagellate blooms. J. Plankton Res. 23, 447–461.
Stockmarr, J., 1971. Tablets with spores used in absolute pollen analysis. Pollen Spores 13, 615–621.
Stramma, L., England, M., 1999. On the water masses and mean circulation of the South Atlantic Ocean. J. Geophys. Res. Oceans 104 (C9), 20863–20883.
Stramma, L., Fischer, J., Reppin, J., 1995. The North Brazil Undercurrent. Deep-Sea Res. I 42, 773–795.
Taylor, F.J.R., 1987. General group characteristics, special features of interest, and a short history of dinoflagellate study. In: Taylor, F.J.R. (Ed.), The Biology of Dinoflagellates. Botanical Monographs. vol. 21. pp. 1–23.
Taylor, F.J.R., Hoppenrath, M., Saldarriaga, J.F., 2007. Dinoflagellate diversity and distribution. In: Foissner, W., Hawksworth, D.L. (Eds.), Protist Diversity and Geographical Distribution. Topics in Biodiversity and Conservation. Springer, Dordrecht, pp. 173–184.
ter Braak, C.J.F., Prentice, I.C., 1988. A theory of gradient analysis. Adv. Ecol. Res. 18, 271–313.
Venancio, I.M., Mulitza, S., Govin, A., Santos, T.P., Lessa, D.O., Albuquerque, A.L.S., Chiessi, C.M., Tiedemann, R., Vahlenkamp, M., Bitcket, T., Schulz, M., 2018. Millennial-to orbital-scale responses of western equatorial Atlantic thermocline depth to changes in the trade wind system since the last Interglacial. Paleoceanogr. Paleoclimatol. 33, 1490–1507.
Verleye, T., Mertens, K., Young, M.D., Dale, B., McMinn, A., Scott, L., Zonneveld, K.A.F., Louwye, S., 2012. Average process length variation of the marine dinoflagellate cyst Operculodinium Centrocarpum in the Tropical and Southern Hemisphere Oceans: assessing its potential as a Palaeosalinity Proxy. Mar. Micropaleontol. 86, 45–58.
Vink, A., Zonneveld, K.A.F., Willems, H., 2000. Organic-walled dinoflagellate cysts in western equatorial Atlantic surface sediments: distributions and their relation to environment. Rev. Palaeobot. Palynol. 112, 247–286.
Vink, A., Brune, A., Höll, C., Zonneveld, K.A.F., Willems, H., 2002. On the response of calcareous dinoflagellates to oligotrophy and stratification of the upper water column in the equatorial Atlantic Ocean. Palaeogeogr. Palaeoclimatol. Palaeoecol. 178 (1–2), 53–66.
Waelbroeck, C., Labeyrie, L., Michel, E., Duplessy, J.C., McManus, J.F., Lambeck, K., Labracherie, M., 2002. Sea-level and deep water temperature changes derived from benthic foraminifera isotopic records. Quat. Sci. Rev. 21 (1–3), 295–305.
Wang, X., Auler, A.S., Edwards, R.L., Cheng, H., 2004. Wet periods in northeastern Brazil over the past 210 kyr linked to distant wet periods in northeastern Brazil over the past 210 kyr linked to distant climate anomalies. Nature 432, 740–743.
Wolff, T., Mulitza, S., Rtihlemann, C., Wefer, G., 1999. Response of the tropical Atlantic thermocline to late Quaternary trade wind changes. Paleoceanography 14 (3), 374–383.
Wolff, E.W., Chappellaz, J., Blunier, T., Rasmussen, S.O., Svensson, A., 2010. Millennial-scale variability during the last glacial: the ice core record. Quat. Sci. Rev. 29 (21 – 22), 2828–2838.
Zhang, Y., Chiessi, C.M., Mulitza, S., Zabel, M., Trindade, R.I.F., Hollanda, M.H.B.M., Dantas, E.L., Govin, A., Tiedemann, R., Wefer, G., 2015. Origin of increased terrigenous supply to the NE South American continental margin during Heinrich Stadial 1 and the Younger Dryas. Earth Planet. Sci. Lett. 432, 493–500.
Zonneveld, K.A.F., Brummer, G.J.A., 2000. (Palaeo-)ecological significance, transport, and preservation of organic-walled dinoflagellate cysts in the Somali Basin, NW Arabian Sea. Deep-Sea Res. Part II: Topic. Stud. Oceanogr. 47, 2229–2256.
Zonneveld, K.A.F., Pospelova, V., 2015. A determination key for modern dinoflagellate cysts. Palynology 39 (3), 387–409.
Zonneveld, K.A.F., Bockelmann, F., Holzwarth, U., 2007. Selective preservation of organic-walled dinoflagellate cysts as a tool to quantify past net primary production and bottom water oxygen concentrations. Mar. Geol. 237, 109–126.
Zonneveld, K.A.F., Versteegh, G.J.M., Kasten, S., Eglinton, T.I., Emeis, K.-C., Huguet, C., Koch, B.P., de Lange, G.J., de Leeuw, J.W., Middelburg, J.J., Mollenhauer, G., Prahl, F., Rethemeyer, J., Wakeham, S., 2010. Selective preservation of organic matter in marine environments; processes and impact on the fossil record. Biogeosciences 7, 483–511.
Zonneveld, K.A.F., Marret, F., Versteegh, G., Bogus, K., Bonnet, S., Bouimetarhan, I., Crouch, E., de Vernal, A., Elshanawany, R., Edwards, L., Esper, O., Forke, S., Grøsfjeld, K., Henry, M., Holzwarth, U., Kielt, J.-F., Kim, S.-Y., Ladouceur, S., Ledu, D., Liang, C., Limoges, A., Londeix, L., Lu, S.-H., Mahmoud, M.S., Marino, G., Matsouka, K., Matthiessen, J., Mildenhal, D.C., Mudie, P., Neil, H.L., Pospelova, V., Qi, Y., Radi, T., Richerol, T., Rochon, A., Sangiorgi, F., Solignac, S., Turon, J.-L., Verleye, T., Wang, Y., Wang, Z., Young, M., 2013. Atlas of modern dinoflagellate cyst distribution based on 2405 data points. Rev. Palaeobot. Palynol. 191 (1–197).